ORIGINAL ARTICLE   **Open Access**

Local structure modification and phase transformation of TiO$_2$ nanoparticles initiated by oxygen defects, grain size, and annealing temperature

Biswajit Choudhury[*] and Amarjyoti Choudhury

Abstract

TiO$_2$ nanoparticles acquire complete crystalline anatase phase on thermal treatment of as-prepared anatase TiO$_2$ at 450°C. Anatase-rutile mixed phase and rutile phase are achieved by annealing anatase TiO$_2$ at 700°C and 950°C respectively. The anatase-rutile mixed phase TiO$_2$ has 87.8% rutile phase. This signifies that the percentage of rutile fraction in mixed phase can be tailored by changing the annealing temperature. As-prepared anatase TiO$_2$ with a crystallite size of 5 nm has a positive strain (η) of 0.0345, which is due to the presence of oxygen defects on the surface and on the grain boundary. Removal of defects releases the strain and relaxes the lattice to its normal state, and thus, a negative strain η of (−) 0.0006 is observed in complete rutile phase. The interface between nearest anatase crystallites and between anatase and rutile crystallites contains oxygen vacancies that act as nucleation site for the growth of rutile nuclei. These oxygen defects are responsible for the broadening of the Raman E_g peak of anatase and for the shortening of the phonon lifetime in a 5-nm-sized anatase nanocrystallite. Removal of defects decreases the Raman peak width and increases the phonon lifetime in a larger rutile crystallite. The long lifetime of phonon in a larger rutile crystallite is due to temperature-dependent anharmonic phonon coupling.

Keywords: Defects; Nucleation; Raman peak; Phonon coupling

Background

Interest in titanium dioxide has been growing because of its wide range of applications in photocatalysis, solar cells, fuel cells, chemical sensors, and glass coating materials for self-cleaning [1-6]. TiO$_2$ exists in the form of three polymorphs: anatase, rutile, and brookite [7]. Out of the three phases, anatase and rutile are known to be the most important and studied polymorphs [8]. Anatase is mainly stable at low temperature, while the rutile phase is stable at high temperature [9]. Since the surface Gibbs free energy of anatase phase is lower than that of rutile phase, TiO$_2$ initially prefers to nucleate into anatase phase rather than into rutile [10]. Due to the different bonding arrangement and structure of the anatase and rutile phases, their applications also differ, e.g., anatase is mainly used in photocatalysis due to its

high photoreactivity and rutile is used as pigments due to its effective light scattering [11]. Although rutile phase has less photocatalytic activity than anatase, the mixed phase of anatase and rutile is known to exhibit enhanced photoactivity [10,12]. Anatase-to-rutile phase transformation is governed by the annealing temperature, compactness of the anatase nanocrystallites, and grain boundary defects [9,11]. Particle arrangement and packing also influence the thermal stability and phase transformation behavior of TiO$_2$ nanoparticles [13]. Zhang et al. [14] proposed that anatase-to-rutile phase transformation is a temperature-dependent process. Penn et al. [15] examined the formation of rutile nuclei on the twin interfaces of anatase particles. Gouma and Mills [16] observed the formation of rutile particles at the expenses of the neighboring anatase particles. Rath et al. [17] studied the role of oxygen defects in the anatase-to-rutile phase transformation of TiO$_2$. Some groups studied the effect of initial crystallite size on the phase transformation of

* Correspondence: biswajit@tezu.ernet.in
Department of Physics, Tezpur University, Napaam 784028, Assam, India

TiO_2 [11,18]. X-ray diffraction and Raman spectra can clearly distinguish the anatase and rutile phases as both of the phases give different diffraction patterns and Raman peaks [17,19,20].

In this article, a careful study is carried out on the role of various factors that change the structure of TiO_2 and initiate the anatase-to-rutile phase transformation. Temperature, crystallite size, and defects induced changes in the local structure, and phase conversion is studied with X-ray diffraction and Raman spectroscopy. Anatase nanocrystallites having small size and high concentration of defects easily undergo phase transformation to rutile. The relation of defects with the Raman line broadening and phonon lifetime is studied, and it is observed that structural defects limit the phonon lifetime in the small anatase nanocrystallites, whereas temperature-dependent anharmonic effect increases phonon lifetime in larger rutile crystallites.

Methods

A sol–gel procedure was adopted to synthesize TiO_2 nanoparticles. Titanium isopropoxide of 7 ml was added to a 100-ml conical flask containing 15 ml of 2-propanol. The solution was stirred for 15 min to get a homogenous solution. After 15 min of stirring, few drops of water were added. Addition of water initiated the ionization of the isopropoxide chain, and the solution adopted a whitish color. Stirring was continued until the solution transformed to a gel. The gel was left for aging for 10 to 12 h. After this aging time, 10 ml of ethanol was added to the titania gel and then sonicated for 10 min to break the gel. The sonicated titania was centrifuged in water and ethanol for 3 to 4 times. The resulting product was kept in an oven at 80°C to get amorphous titania. The amorphous titania was heat treated at 200°C for 3 h to increase the crystallinity. This sample was labeled as Ti200. Ti200 was separated into four parts. One part remained as Ti200, while the other three parts were annealed for 3 h at 450°C (Ti450), 700°C (Ti700), and 950°C (Ti950), respectively.

X-ray diffraction pattern of the prepared samples were studied with a Rigaku Miniflex X-ray diffractometer (Rigaku Corporation, Tokyo, Japan) equipped with intense Cu Kα radiation (λ = 0.154 nm). The scanning rate was 1°/min and the step size was 0.05°. Transmission electron microscope (TEM) images were taken with a JEOL JEM 2100 transmission electron microscope (JEOL Ltd., Tokyo, Japan), operating at an accelerating voltage of 200 kV. The bonding interaction in the TiO_2 nanoparticles was studied with Nicolet Fourier transform infrared spectroscopy (FTIR; Thermo Scientific, Madison, WI, USA). Room-temperature Raman spectra were taken using a Renishaw inVia Raman spectrometer (Renishaw, Wotton-under-Edge, UK) at a spectral resolution of 0.3 cm^{-1}.
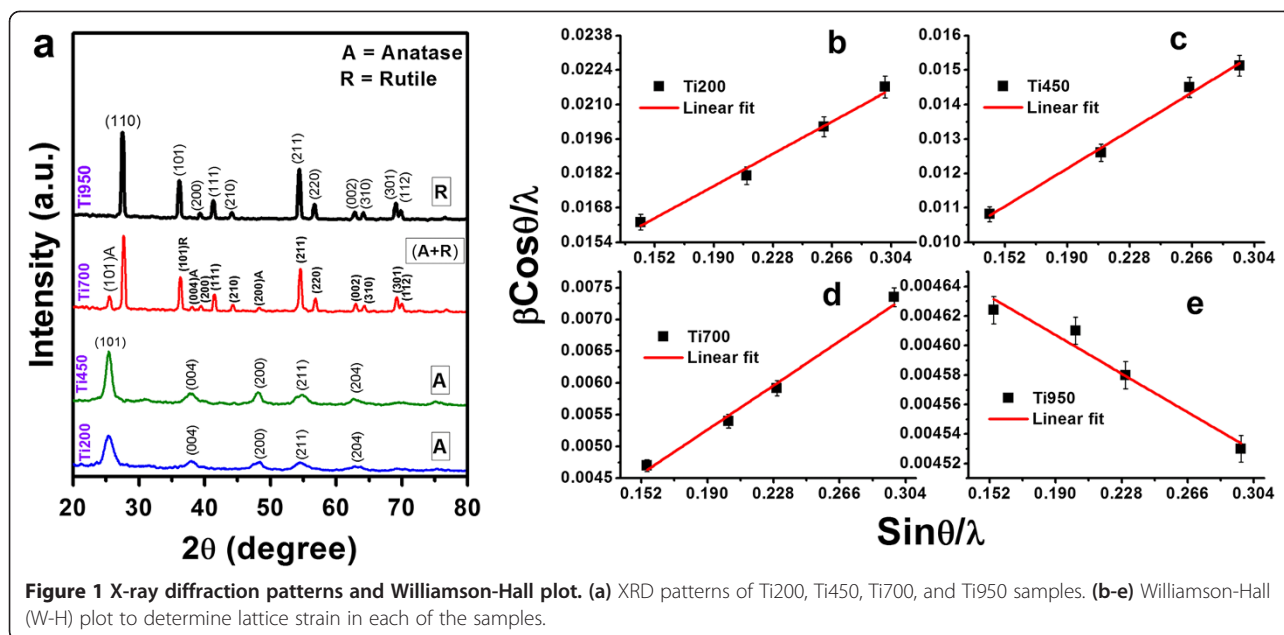
Results and discussion

X-ray diffraction study

Figure 1a represents the X-ray diffraction (XRD) pattern of the entire TiO_2 systems. Diffraction patterns of Ti200 and Ti450 correspond to the tetragonal anatase phase of TiO_2 with space group $I4_1/amd$ (JCPDS 78–2486). Ti950 adopts complete a rutile phase with space group $P4_2/mnm$ (JCPDS 21–1276). However, an anatase-rutile mixed phase is found in Ti700. The percentages of rutile (W_R) in Ti700 and Ti950 are calculated using Equation 1 [11]:

$$W_R = \frac{I_R}{0.884\,I_A + I_R} \qquad (1)$$

where I_A and I_R are the diffraction peak intensities of anatase (101) and rutile (110) peaks. Gaussian fitting of these peaks gives the magnitudes of I_R and I_A. The values of I_A and I_R are inserted in the above equation. The resultant W_R values are 87.8% and 98% in Ti700 and Ti950, respectively.

Crystallite size of the samples is calculated using Scherrer's equation, $d = 0.9\lambda/\beta\cos\theta$, where d is the crystallite size, β is the full width at half maximum (FWHM), λ is the wavelength of X-ray radiation, and θ is the diffraction angle. Table 1 shows the variation of crystallite size for samples annealed at different temperatures. As evident from Figure 1a and from Table 1, the diffraction peaks of Ti200 are broad and correspond to the anatase phase of TiO_2 having a crystallite size of 5 nm. The broad diffraction peaks arise, owing to the presence of a high fraction of atoms on the amorphous grain boundary containing defects. The defects in this region produce a strain and prevent growth of the nanocrystallite. Complete grain growth to anatase occurs when Ti200 is annealed at 450°C with simultaneous enhancement in the crystallinity in the material. No phase conversion to rutile is observed at this temperature. Anatase-rutile mixed phase is seen by annealing Ti200 at 700°C. At this temperature, the defects at the interface boundary are removed and a major fraction of anatase is converted to rutile, resulting in 87.8% rutile phase in the mixed phase Ti700. Annealing in air at 950°C removes grain boundary defects and increases the grain size with a majority of 98% rutile phase. Therefore, it is observed that annealing temperature is one factor that facilitates anatase-to-rutile phase transformation. Presence of 87.8% rutile phase in Ti700 indicates that phase conversion has started at a temperature lower than 700°C. Therefore, the desired fraction of rutile phase can be obtained by changing the annealing temperature of anatase TiO_2. It is mentioned that defects present on the grain boundary produce lattice strain and prevent grain growth, and therefore, to confirm this statement, the lattice strain is determined for

Figure 1 X-ray diffraction patterns and Williamson-Hall plot. (a) XRD patterns of Ti200, Ti450, Ti700, and Ti950 samples. **(b-e)** Williamson-Hall (W-H) plot to determine lattice strain in each of the samples.

each sample by adopting the Williamson-Hall (W-H) equation [21]:

$$\frac{\beta\cos\theta}{\lambda} = \frac{1}{D} + \eta\frac{\sin\theta}{\lambda}. \quad (2)$$

In Equation 2, λ is the wavelength of X-ray radiation and β and θ are the FWHM and diffraction angle of the first four intense diffraction peaks of anatase, anatase-rutile mixed, and rutile phases. D is the effective crystallite size considering lattice strain, and η is the effective value of lattice strain. $\beta\cos\theta/\lambda$ is plotted against $\sin\theta/\lambda$, and after linear fitting, the intercept gives the value of D and the slope gives the value of η. Figure 1b,c,d,e illustrates the W-H plot of all the TiO$_2$ samples. The magnitude of lattice strain of each sample is inserted in Table 1. As evident from Table 1, Ti200 exhibits the highest lattice strain, whereas Ti950 has the lowest. The high lattice strain in Ti200 is due to the presence of an excess number of atoms and defects on the amorphous grain boundary. These defects and excess atoms produce a stress field in this region and impose a strain in

the system [22]. Positive strain indicates that the system is under tensile strain. The crystallite size increases and the defects are gradually removed when Ti200 is subjected to heat treatment at 450°C, 700°C, and 950°C, respectively. Removal of grain boundary defects and increase of crystallite size reduce the stress field in this region, resulting in the release of lattice strain [22,23]. Therefore, annealing temperature is one factor that initiates the phase transformation from anatase to rutile [24-26]. Apart from annealing temperature, the other factors which initiate the anatase-to-rutile phase conversion are crystallite size and defects. Shah and his groups reported that anatase TiO$_2$ with small crystallite size needs less activation energy for undergoing phase conversion to rutile [11]. Now, whether the phase conversion occurs by surface or interface nucleation depends on the packing density of the nanoparticles [13]. Small nanoparticles have a large number of particle-particle contacts per unit volume, and therefore, interface nucleation is more feasible than surface nucleation [27]. Because of the presence of a large number of nucleation sites, these small anatase nanocrystallites cross low potential barrier for undergoing conversion to rutile [27]. As the size of Ti200 is small (4 nm), this nanocrystallite can easily change to rutile by undergoing interface nucleation. Since phase transformation is supposed to take place at the interfaces of the neighboring anatase nanocrystallites, increase in the distance among them decreases the phase transformation rate [28].

The other factor which facilitates the anatase-to-rutile phase conversion is oxygen defects [17,29]. Lee et al. stated that rutile nucleation is most prominent at the amorphous interfaces of neighboring anatase where the

Table 1 Crystallite size, lattice strain, Raman E_g peak width, and phonon lifetime of entire TiO$_2$ samples

Sample	Annealing temperature (°C)	Crystallite size (nm)	Lattice strain	Raman line width E_g (cm^{-1})	Phonon lifetime (ps)
Ti200	200	5	0.0345	29.7	0.178
Ti450	450	8	0.0290	21.8	0.243
Ti700	700	18	0.0183	19.2	0.276
Ti950	950	23	−0.0006	18.1	0.293

strain is very high [26]. In the W-H plot, it is seen that Ti200 possesses the highest lattice strain and it is stated that oxygen defects on the grain boundary is the reason for this strain. Since the crystallite size of Ti200 is small, these oxygen defects are closely packed and they interact with each other, creating a nucleation site for the formation of rutile nuclei. Some of these oxygen vacancies are removed by air annealing of Ti200 and 450°C, since the system attains complete anatase phase. Although crystallite defects are somehow removed in Ti450, these defects are again generated at the interface between anatase and rutile when anatase is slowly transforming to rutile at 700°C. Although anatase and rutile have the same basic TiO_6 octahedra, the arrangement of atoms in this basic unit changes when anatase transforms to rutile [30]. During the process of the phase conversion from anatase to rutile, the TiO_6 octahedra undergo distortion on heat treatment, and then finally, breaking and reforming of new Ti-O bonds take place at the interface and at the grain interior [29]. Lattice distortion and breaking of Ti-O bonds at 700°C result in the removal of oxygen ions and creation of defects along with reformation of new Ti-O bonds in the rutile phase. Therefore, defects, particularly oxygen vacancies, may serve as a nucleation site to facilitate the formation of rutile phase [17,29]. Entire defects undergo interface nucleation process for the formation of rutile phase, and finally, at 950°C, the Ti-O bonds are fully reconstructed and the Ti950 becomes nearly free of crystalline defects. Temperature-dependent grain growth and anatase-to-rutile phase conversion of TiO_2 involve creation of interface defects, atomic migration from the interface to grain interior, and then finally reconstruction of a new crystalline phase and removal of defects. Annealing, however, may not heat up the entire Ti200 grains equally. Those grains which absorb maximum heat will grow in size at a faster rate than those which absorbs less heat energy. In this process, some grains will grow in size at the expense of some shrinking grains which absorbs less thermal energy. Thermal treatment ruptures the interface boundary between as-grown grains and shrinking grains and results in the detachment of the atoms from the interface boundary. The detached atoms undergo migration from the interface of the shrinking grain and form new bonds with the growing grain [31]. The microscopic driving force involved in the growth of grains and for the shrinking of grain is equal, and it is given by [31]

$$\Delta G_d^S = \Delta G_d^G = 2\gamma_g \left(\frac{1}{r_a} - \frac{1}{r_b} \right)$$ (3)

where ΔG_d^S and ΔG_d^G are the driving force for shrinking of grain and for the growth of grain, r_a is the radius of

shrinking grain (a) and r_b is that of growing (b) grain, respectively, and γ_g is the energy of the grain boundary. Since Ti200 has high concentration of defects on the grain boundary, these defects produce some steps or kinks to which the atoms from the shrinking grain can easily jump. This process lowers the energy for the migration of atoms from the shrinking grain to the growing grain. A schematic representation of the formation of larger rutile particles from the starting anatase particles is shown in Figure 2.

TEM analysis
Figure 3a,b shows the TEM images of Ti200 and Ti450, respectively. As shown in Figure 3a,b, the particles are agglomerated. Statistical analyses of the micrographs depict the average size of the nanoparticles. Ti200 has an average size of 5 nm. The particle size increases to 7 nm in Ti450. The interfaces of the closely associated anatase nanoparticles act as nucleation sites for undergoing phase transformation to rutile. Heat treatment of Ti200 at 700°C results in the growth of the nanoparticles. However, as it is seen in Ti700, some small-sized particles are also present along with large rutile TiO_2 particles (Figure 3c). Ti950 has rutile phase with particles having a large diameter (Figure 3d). The average particle size becomes 30 nm in Ti700 and 40 nm in Ti950. Ti700 also contains some average 10-nm-sized nanoparticles. Penn
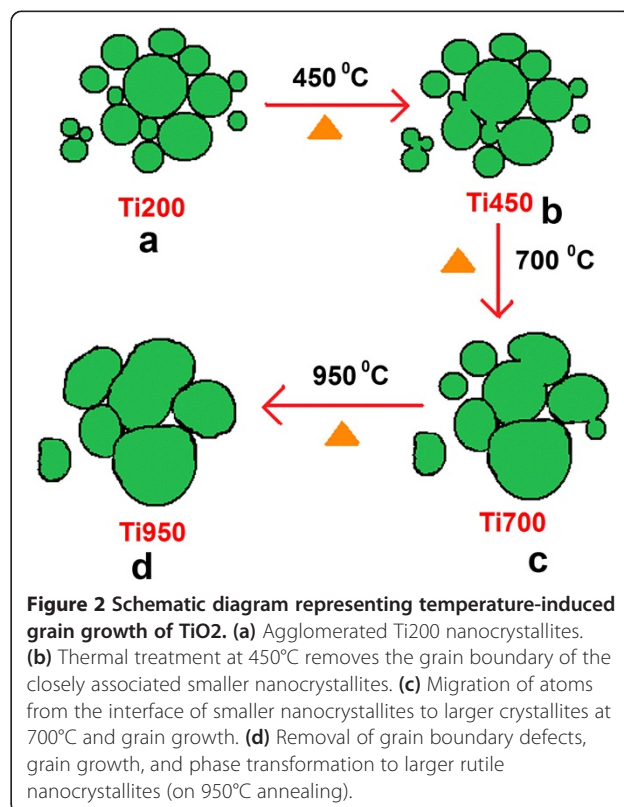

Figure 2 Schematic diagram representing temperature-induced grain growth of TiO2. (a) Agglomerated Ti200 nanocrystallites. **(b)** Thermal treatment at 450°C removes the grain boundary of the closely associated smaller nanocrystallites. **(c)** Migration of atoms from the interface of smaller nanocrystallites to larger crystallites at 700°C and grain growth. **(d)** Removal of grain boundary defects, grain growth, and phase transformation to larger rutile nanocrystallites (on 950°C annealing).
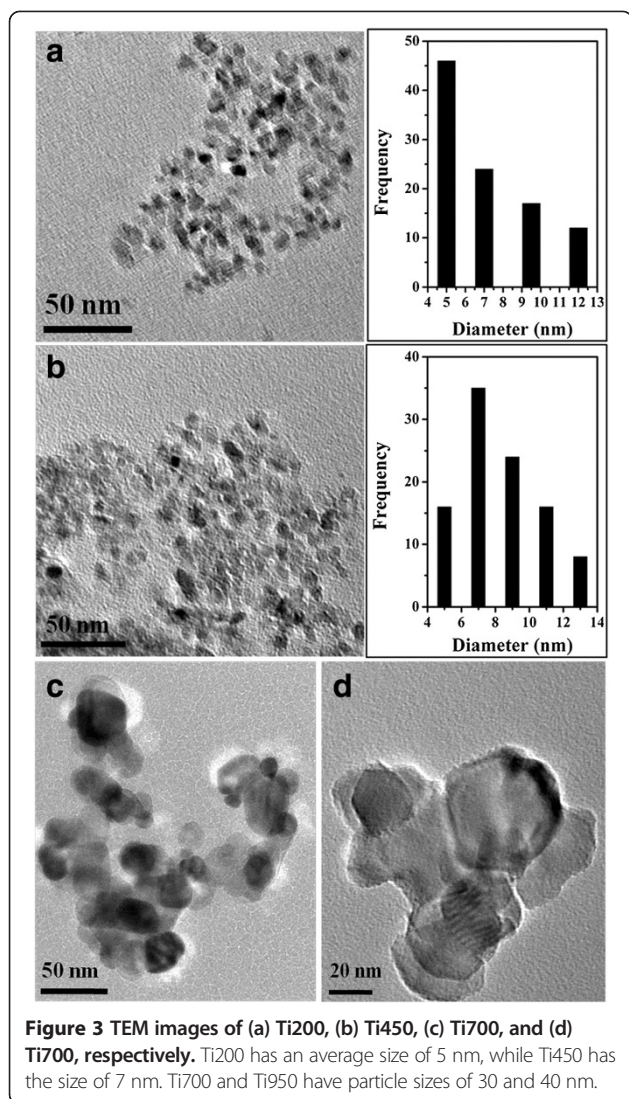
Figure 3 TEM images of (a) Ti200, (b) Ti450, (c) Ti700, and (d) Ti700, respectively. Ti200 has an average size of 5 nm, while Ti450 has the size of 7 nm. Ti700 and Ti950 have particle sizes of 30 and 40 nm.

et al. [15] in their HRTEM study of this polymorphic phase transformation suggested that anatase-to-rutile phase conversion occurs at the twin boundaries of the interface of the adjacent anatase nuclei. Kim et al. [32] reported that the distorted region at the interfaces of the neighboring anatase nuclei may act as nucleation site for phase transformation. There is a difference in the sizes determined by TEM and XRD, particularly in the case of Ti700 and Ti950. The size determined by XRD is the size of the coherently scattering domain coming from single crystals of parallel lattice planes [33,34].

The diffraction pattern gives an average size of the entire nanoparticles present within the sample, while TEM gives particle size distribution and represents direct visualization of the different types of nanoparticles present [32-34]. The magnitude of crystallite and particle sizes matches with each other, only when the particles are monodispersed, single crystals, and hard spheres. Disagreement with these

conditions results in the deviation of the sizes, measured by the two techniques [34].

FTIR study

Figure 4 shows the FTIR curves of Ti200, Ti450, Ti700, and Ti950. Each curve exhibits a peak at approximately 1,630 cm^{-1} whose intensity decreases with annealing temperature. This peak is mainly attributed to the H-O-H bending vibration of physisorbed water [35]. Nanoparticles with high specific surface area can adsorb many molecules of water on the specific active sites on the surface and can form Ti^{4+}-OH$_2$ on the surface [36]. Adsorption of these water molecules evolves considerable heat and helps in the transition of TiO$_2$ from anatase to rutile [36,37].

The adsorbed water lowers the temperature for anatase-to-rutile phase transition [37]. As the sample is annealed at 450°C, 700°C, and 950°C, the H-O-H bonds, attached to Ti^{4+}, are broken up and the negatively charged O^{2-} takes part in the formation of new bonds with the Ti^{4+} ions. Ding et al. [10] studied that the rutile content increases with the water concentration and that these water molecules at the surface and in the interface help in the aggregation of the nanoparticles. As annealing temperature increases, the water molecules at the interface and on the surface, attached to Ti^{4+}, are dissociated, forming new Ti-O bonds at the interface. Jose et al. [36] have studied that the heat evolved during adsorption of water on activated TiO$_2$ surfaces and during annealing can help in the formation of aggregated TiO$_2$ particles and formation of new Ti-O bonds. In Ti200, the small crystallite size with large surface-to-volume ratio can hold many water molecules. These molecules help in the formation of rutile nuclei. Increase in annealing temperature results in the increase in crystallite size, thereby decreasing the surface area for adsorption of water. That is why the intensity of the water band is decreasing with thermal treatment.

Raman spectroscopy study

Raman spectra of the entire TiO$_2$ samples are shown in Figure 5a. Anatase TiO$_2$ has six Raman-active modes and three infrared (IR)-active modes. The optical phonon mode at the Γ-point of the Brilliouin zone (BZ) is presented by [38]

$$\Gamma = A_{1g}(\text{R}) + 2B_{1g}(\text{R}) + 3E_g(\text{R}) + B_{2u}(\text{IR}) \\ + A_{2u}(\text{IR}) + 2E_u(\text{IR}). \qquad (4)$$

For rutile TiO$_2$, factor group analysis gives four Raman-active modes at $k = 0$ in BZ [39].

$$\Gamma = A_{1g}(\text{R}) + A_{2g} + A_{2u}(\text{IR}) + B_{1g}(\text{R}) + B_{2g}(\text{R}) \\ + 2B_{1u} + E_g(\text{R}) + 3E_u(\text{IR}) \qquad (5)$$

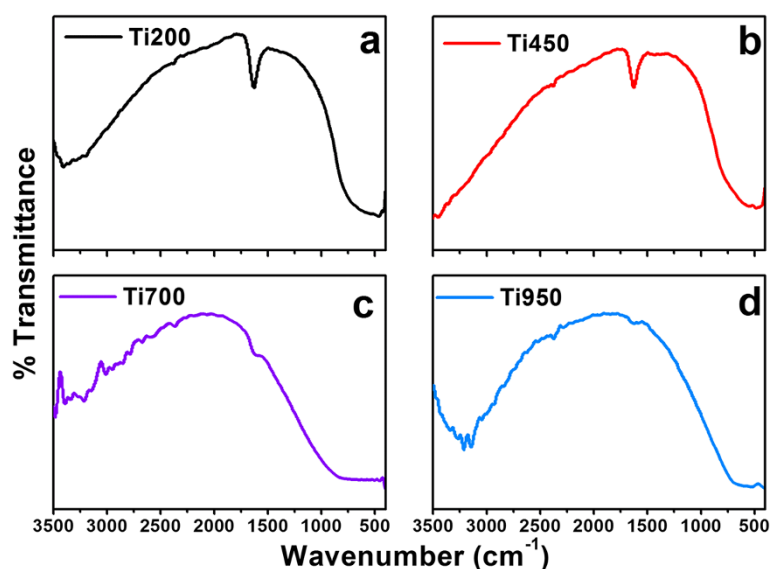The four vibrations ($A_{1g} + B_{1g} + B_{2g} + E_g$) are Raman active and the rest are IR active.

Figure 4 FTIR spectra of (a) Ti200, (b) Ti450, (c) Ti700, and (d) Ti950.

Ti200 and Ti450 exhibit Raman peaks corresponding to the anatase phase of TiO$_2$. In these samples, an intense E_g peak appears at 144 cm^{-1}, followed by low intense B_{1g} (A_{1g} + B$_{1g}$) and E_g peaks at 410 cm^{-1}, 520 cm^{-1}, and at 640 cm^{-1}, respectively [19,28]. In the case of Ti700, the E_g peak of anatase remains at 144 cm^{-1}, while rutile peaks appear at 240, 450, and 620 cm^{-1}, respectively [40,41]. The Raman peak at 240 cm^{-1} is the compound vibration peak due to the multiple phonon scattering process [41]. In Ti950, the intensity of 144 cm^{-1} is decreased and Raman peaks analogous to rutile TiO$_2$ predominates [39-41]. Lattice strain, defects, and crystallite size have a profound effect in the shifting, peak broadening, and on the intensity of the Raman peaks [42,43].

For pure crystal, the phonon contribution comes from the center of the Brillouin zone, at q = 0 [20,41,42]. However, for small nanocrystallites, the phonon dispersion takes on phonon contribution from the entire Brillouin zone [43,44]. The breaking of the phonon selection rule influences the Raman line shape, position, etc. [44]. Positive phonon dispersion from the zone center will lead to asymmetric broadening, blueshift, and reduction in the intensity of the Raman peak [42]. The intensity of first-order Raman scattering for nanocrystals of diameter d is

$$I(\omega,d) = \int\limits_{BZ} \frac{|c\,(q,d)|^2}{[\omega\text{-}\omega(q)]^2 + \left(\frac{\Gamma_0}{2}\right)^2} d^3q \qquad (6)$$

where c (q,d) is the Fourier transformation of the confinement function, $\omega(q)$ is the phonon dispersion curves, and Γ_0 is the natural line width [42]. The size of the nanocrystals and presence of defects have a profound effect on the Raman peak position, line width, etc. To study the effect of size, defects, and temperature on the position and width of the Raman peak, the E_g Raman peak
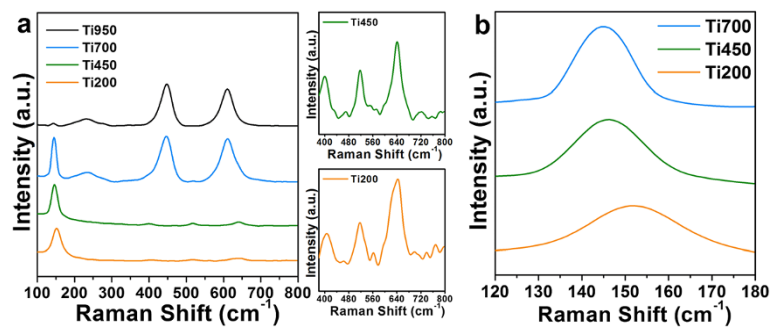

Figure 5 Raman spectra and red shifting. (a) Room-temperature Raman spectra of Ti200, Ti450, Ti700, and Ti950 samples. The right side of this figure shows the Raman peak of Ti200 and Ti450 in the 380- to 800-cm^{-1} range. **(b)** Red shifting of the E_g peak of Ti450 and Ti700 compared to that of Ti200.

is considered. Figure 5b shows the E_g mode of Ti200, Ti450, Ti700, and Ti950, respectively. The intensity of this mode increases as the temperature increases, and the anatase undergoes phase transformation to rutile. Low intense E_g mode at 144 cm^{-1} is also present in Ti950. This indicates that Ti950 contains a small percentage of anatase phase also. The E_g mode of each sample is Lorentzian fitted with a correctness of r^2 = 0.9985. The line width of the E_g Raman peak is inserted in Table 1.

Oxygen defects also affect the Raman line shape and position [43-45]. The positions of the E_g peak of Ti450 and Ti700 are shifted to a lower wave number compared to that of Ti200 (Figure 5b). The E_g peak of bulk anatase appears at 144 cm^{-1} [29]. In Ti200, both phonon confinement and oxygen defects result in the broadening and shifting of the E_g line to a higher wave number. Temperature treatment, however, decreases the defects, increases the crystallite size, and gradually shifts the E_g peak from 151 cm^{-1} (in Ti200) to 144 cm^{-1} (in Ti950). In Raman modes, mostly oxygen atoms move during vibration [39]. Since temperature treatment changes the local coordination of oxygen surrounding Ti^{4+}, conversion of anatase to rutile results in the rearrangement of TiO$_6$ octahedra and shifting in the position of Raman-active peaks. Table 1 shows that the line width of the Raman E_g peak is decreasing with annealing temperature. Three phonon processes contribute to the broadening of the E_g mode [46]. As explained, the width of the Raman peak is influenced by strain, oxygen vacancies, temperature, size, etc. The temperature-dependent Raman line width is represented by the equation [44]

$$\Gamma\,(T) = \Gamma_1 + \Delta\Gamma\,(T). \qquad (7)$$

The first term in Equation 7 is due to other types of broadening such as instrumental broadening, defects, phonon confinement, etc. $\Delta\Gamma\,(T)$ is from three-phonon coupling decay or temperature-dependent intrinsic line width of the first-order phonon. In Ti200, the structural defects are considerably high along with strong phonon confinement due to the small size of the nanocrystallite. In Ti450, the structural defects are slightly removed. The line broadening in Ti200 and Ti450 is due to the presence of structural defects. The temperature-dependent anharmonic term is not prominent here. In Ti700, the crystallite size increases along with reduction in the amount of structural defects. In Ti950, anatase is transformed to rutile. At this temperature, most of the structural defects are removed and the crystallite size and Raman peak position approaches to that of bulk TiO$_2$. The position of the E_g Raman peak of Ti950 is similar to that of bulk TiO$_2$. In this sample, the anharmonic coupling term is more prominent and the first term becomes

zero [44]. The phonon lifetime is calculated considering peak broadening of the E_g peak of each sample. The energy-time uncertainty relation for the determination of phonon lifetime is $\Delta E/\hbar = 1/\tau = 2\pi c\Gamma$, where ΔE is the uncertainty in the energy of phonon mode, $\hbar$ is the reduced plank constant, Γ is the FWHM of the Raman peak, and τ is the phonon lifetime [41,46]. The calculated phonon lifetime of each sample is inserted in Table 1. The phonon lifetime decreases as the sample transforms from anatase to rutile. The phonon lifetime is shorter in Ti200 and Ti450 due to phonon confinement in the small nanocrystallite [46]. Since the amount of defects in Ti200 is very high, the confined phonon may undergo elastic and inelastic scattering process with crystal defects limiting the phonon lifetime. As temperature increases and the crystal size increases, the phonon density increases, and the temperature-dependent anharmonic phonon coupling increases. This finally increases the decay time or the lifetime of the phonons [46]. Therefore, in larger crystals of Ti950, the phonon decays with a longer lifetime. Mali et al. [41] also observed an increase in phonon lifetime with the decrease of Raman line width in rutile TiO$_2$ particles. They observed that the as-grain size increases the FWHM of the Raman A_{1g} peak and that the E_g peak decreases with the simultaneous increase in phonon lifetime.

Anatase is known to be an efficient material for photocatalysis, and in recent days, anatase-rutile mixed phase has drawn attention for heterogeneous photocatalysis. Presence of defects at the interface between anatase and rutile is one of the reasons for the enhanced photocatalytic activity of mixed phase TiO$_2$ [47]. From the above discussion on the phase transformation from anatase to rutile, it is inferred that the interface defects are mostly oxygen vacancies and that these defects not only trap the photoexcited electrons but also make these carriers available for taking part in photocatalysis. Moreover, the band alignment in the anatase-rutile mixed phase also enhances the photocatalytic activity. Anatase has a band gap of 3.2 eV, whereas the band gap of rutile is 3.0 eV; thus, the carriers can move from the conduction band of anatase to the conduction band of rutile [30]. Lei et al. stated that anatase-rutile mixed phase with 60% anatase can show better photocatalytic activity than individual anatase or rutile TiO$_2$ [48]. Although photocatalytic activity is not studied in the work, it can be suggested that by changing the annealing temperature, the desired anatase-rutile mixed phase composition can be obtained in which the material is expected to show good photocatalytic activity.

Conclusions

In conclusion, crystallite size, oxygen defects, temperature, etc. initiate the nucleation and growth of rutile from initially grown anatase TiO$_2$ nuclei. Initially grown small

anatase Ti200 has high content of defects on the interface of the attached anatase nuclei. These defects initiate the growth of rutile TiO$_2$. Phase transformation rearranges the bonding arrangement and introduces many defects in the anatase-rutile mixed phase TiO$_2$. X-ray diffraction, transmission electron microscopy, FTIR, and Raman spectroscopy clearly distinguish the basic structure of anatase and rutile, their sizes, the adsorbed species on the surface, and presence of defects. It is observed that anatase-rutile mixed phase with 87% rutile content has very high concentration of defects at the interface. These defects act as a nucleation site for the growth of rutile particles at 950°C. Therefore, the defect content at the interface in the mixed phase can be tailored by changing the annealing temperature. There is an inverse relationship between the Raman line width and phonon lifetime. Ti200 has a broad Raman line width and a short phonon lifetime, owing to the presence of defects. However, with the decrease of oxygen defects and with the increase of annealing temperature and crystallite size, the Raman line width decreases and phonon lifetime increases.

Nomenclature

H   strain
β full width at half maximum
λ wavelength of X-ray radiation
θ diffraction angle
Γ (T)   line width of Raman peak at a particular temperature
τ phonon lifetime.

Competing interests
The authors declare that they do not have any competing interests.

Authors' contributions
BC designed the objective of the work, synthesized and characterized the samples and drafted the manuscript. AC participated in the development of the idea of the work and approved the final draft of the manuscript.

References
1. Sui, R, Rizkalla, AS, Charpentier, PA: FTIR study on the formation of TiO$_2$ nanostructures in supercritical CO$_2$. J Phys Chem B 110, 16212–16218 (2006)
2. Anpo, M, Takeuchi, M: The design and development of highly reactive titanium oxide photocatalysts operating under visible light irradiation. J Catal 216, 505–516 (2003)
3. Song, MY, Kim, DK, Ihn, KJ, Jo, SM, Kim, DY: Electrospun TiO$_2$ electrodes for dye-sensitized solar cells. Nanotechnology 15, 1861–1865 (2004)
4. Liu, Y, Li, J, Zhou, B, Chen, H, Wang, Z, Cai, W: A TiO$_2$-nanotube-array-based photocatalytic fuel cell using refractory organic compounds as substrates for electricity generation. Chem Commun 47, 10314–10316 (2011)
5. Qiu, J, Zhang, S, Zhao, H: Recent applications of TiO$_2$ nanomaterials in chemical sensing in aqueous media. Sens Actuators B 160, 875–890 (2011)
6. Valtierra, JM, Reyes, CF, Ortiz, JR, Martinez, GC: Self-cleaning test of doped TiO$_2$-coated glass plates under solar exposure. Ind Eng Chem Res 48, 598–606 (2009)
7. Coronado, DR, Gattorno, GR, Pesqueira, ME, Cab, C, Coss, R, Oskam, RG: Phase pure TiO$_2$ nanoparticles: anatase, brookite and rutile. Nanotechnology 19, 145605 (2008)
8. Shi, J, Chen, J, Feng, Z, Chen, T, Lian, Y, Wang, X, Li, C: Photoluminescence characteristics of TiO$_2$ and their relationship to the photoassisted reaction of water/methanol Mixture. J Phys Chem C 111, 693–699 (2007)
9. Madras, G, McCoy, BJ, Navrotsky, A: Kinetic model for TiO$_2$ polymorphic transformation from anatase to rutile. J Am Ceram Soc 90, 250–255 (2007)
10. Ding, K, Miao, Z, Hu, B, An, G, Sun, Z, Han, B, Liu, Z: Study on the anatase to rutile phase transformation and controlled synthesis of rutile nanocrystals with the assistance of ionic liquid. Langmuir 26, 10294–10302 (2010)
11. Li, W, Ni, C, Lin, H, Huang, CP, Shah, SI: Size dependence of thermal stability of TiO$_2$ nanoparticles. J Appl Phys 96, 6663–6668 (2004)
12. Scotti, R, Bellobono, IR, Canevali, C, Cannas, C, Catti, M, D'Arienzo, M, Musinu, A, Polizzi, S, Sommariva, M, Testino, A, Morazzoni, F: Sol–gel pure and mixed phase titanium dioxide for photocatalytic purposes: relations between phase composition, catalytic activity, and charge-trapped sites. Chem Mater 20, 4051–4061 (2008)
13. Wang, CC, Ying, JY: Sol–gel synthesis and hydrothermal processing of anatase and rutile titania nanocrystals. Chem Mater 11, 3113–3120 (1999)
14. Zhang, H, Banfield, JF: Phase transformation of nanocrystalline anatase-to-rutile via combined interface and surface nucleation. J Mater Res 15, 437–448 (2000)
15. Penn, RL, Banfield, JF: Formation of rutile nuclei at anatase (112) twin interfaces and the phase transformation mechanism in nanocrystalline titania. Am Mineral 84, 871–876 (1999)
16. Gouma, P, Mills, MJ: Anatase-to-rutile transformation in titania powders. J Am Ceram Soc 84, 619–622 (2001)
17. Rath, C, Mohanty, P, Pandey, AC, Mishra, NC: Oxygen vacancy induced structural phase transformation in TiO$_2$ nanoparticles. J Phys D Appl Phys 42, 205101–205106 (2009)
18. Zhang, H, Banfield, JF: Understanding polymorphic phase transformation behavior during growth of nanocrystalline aggregates: insights from TiO$_2$. J Phys Chem B 104, 3481–3487 (2000)
19. Zhang, WF, He, YL, Zhang, MS, Yin, Z, Chen, Q: Raman scattering study of anatase TiO$_2$ nanocrystals. J Phys D Appl Phys 33, 912–916 (2000)
20. Skryshevskyy, VA, Dittrich, T, Rappich, J: Infrared-active defects in a TiO$_2$ mixture of coexisting anatase and rutile phases. Phys Stat Sol A 201, 157–161 (2004)
21. Choudhury, B, Choudhury, A: Ce^{3+} and oxygen vacancy mediated tuning of structural and optical properties of CeO$_2$ nanoparticles. Mater Chem Phys 131, 666–671 (2012)
22. Qin, W, Szpunar, JA: Origin of lattice strain in nanocrystalline materials. Phil Mag Lett 85, 649–656 (2005)
23. Moghaddam, HM, Nasirian, S: Dependence of activation energy and lattice strain on TiO$_2$ nanoparticles? Nanoscience Methods 1, 201–212 (2012)
24. Gnaser, H, Losch, J, Orendorz, A, Ziegler, C: Temperature-dependent grain growth and phase transformation in mixed anatase-rutile nanocrystalline TiO$_2$ films. Phys Stat Solidi A 208, 1635–1640 (2011)
25. Yanagisawa, K, Ovenstone, J: Crystallization of anatase from amorphous titania using the hydrothermal technique: effects of starting material and temperature. J Phys Chem B 103, 7781–7787 (1999)
26. Lee, GH, Zuo, JM: Growth and phase transformation of nanometer-sized titanium oxide powders produced by the precipitation method. J Am Ceram Soc 87, 473–479 (2004)
27. Zhang, J, Xu, Q, Li, M, Feng, Z, Li, C: UV Raman spectroscopic study on TiO$_2$. II. Effect of nanoparticle size on the outer/inner phase transformation. J Phys Chem C 113, 1698–1704 (2009)
28. Zhang, J, Li, M, Feng, Z, Chen, J, Li, C: UV Raman spectroscopic study on TiO$_2$. I. Phase transformation at the surface and in the bulk. J Phys Chem B 110, 927–935 (2006)
29. Shannon, RD: Phase transformation studies in TiO$_2$ supporting different defect mechanism in vacuum reduced and hydrogen reduced rutile. J Appl Phys 35, 3414–3416 (1964)
30. Scanlon, DO, Dunnill, CW, Buckeridge, J, Shevlin, SA, Logsdail, AJ, Woodley, SM, Catlow, CR, Powell, MJ, Palgrave, RG, Parkin, IP, Watson, GW, Keal, TW, Sherwood, P, Walsh, A, Sokol, AA: Band alignment of rutile and anatase TiO$_2$. Nat Mater 12, 798–801 (2013)
31. Dillon, SJ, Harmer, MP: Diffusion controlled abnormal grain growth in ceramics. Materials Res Forum 558–559, 1227–1236 (2007)

32. Kim, KH, Park, H, Ahn, JP, Lee, JC, Park, JK: HRTEM study of phase transformation from anatase to rutile in nanocrystalline TiO_2 particles. Mater Sci Forum **534**, 65–68 (2007)
33. Borchert, H, Shevchenko, E, Robert, A, Mekis, I, Kornowski, A, Grubel, G, Weller, H: Determination of nanocrystal sizes: a comparison of TEM, SAXS, and XRD studies of highly monodisperse CoPt3 particles. Langmuir **21**, 1931–1936 (2005)
34. Baalousha, M, Nam, YJ, Cole, PA, Gaiser, B, Fernandes, TF, Hriljac, JA, Jepson, MA, Stone, V, Tyler, CR, Lead, JR: Characterisation of cerium oxide nanoparticles—part 1: size measurements. Environ Toxicol **31**, 983–993 (2012)
35. Takahashi, K, Hiroharu, Y: Analysis of surface OH groups on TiO_2 single crystal with polarization modulation infrared external reflection spectroscopy. J Phys Chem C **113**, 20322–20327 (2009)
36. Amores, JMG, Escribano, VS, Busca, G: Anatase crystal growth and phase transformation to rutile in high-area TiO_2, MoO_3–TiO_2 and other TiO_2-supported oxide catalytic systems. J Mater Chem **5**, 1245–1249 (1995)
37. Ha, PS, Youn, HJ, Jung, HS, Hong, KS, Park, YH, Ko, KH: Anatase-rutile transition of precipitated titanium oxide with alcohol rinsing. J Colloid Interface Sci **223**, 16–20 (2000)
38. Brojcin, MG, Scepanovic, MJ, Mitrovic, ZD, Hinic, I, Matovic, B, Stanisic, G, Popovic, Z: Infrared study of laser synthesized anatase TiO_2 nanopowders. J Phys D Appl Phys **38**, 1415–1420 (2005)
39. Ocana, M, Fornes, V, Ramos, JV, Serna, CJ: Factors affecting the infrared and Raman spectra of rutile powders. J Solid State Chem **75**, 364–372 (1988)
40. Swamy, V, Muddle, BC, Dai, Q: Size-dependent modifications of the Raman spectrum of rutile TiO_2. Appl Phys Lett **89**, 163118–163120 (2006)
41. Mali, SM, Betty, CA, Bhosale, PN, Patil, PS: Hydrothermal synthesis of rutile TiO_2 with hierarchical microspheres and their characterization. Cryst Engg Comm **13**, 6349–6351 (2011)
42. Georgescu, D, Baia, L, Ersen, O, Baia, M, Simon, S: Experimental assessment of the phonon confinement in TiO_2 anatase nanocrystallites by Raman spectroscopy. J Raman Spect **43**, 876–883 (2012)
43. Sahoo, S, Arora, AK, Sridharan, V: Raman line shapes of optical phonons of different symmetries in anatase TiO_2 nanocrystals. J Phys Chem C **113**, 16927–16933 (2009)
44. Zhu, KR, Zhang, MS, Qiang, C, Zhen, Y: Size and phonon-confinement effects on low-frequency Raman mode of anatase TiO_2 nanocrystal. Phys Lett A **340**, 220–227 (2005)
45. Gao, K: Strong anharmonicity and phonon confinement on the lowest-frequency Raman mode of nanocrystalline anatase TiO_2. Phys Stat Sol B **244**, 2597–2604 (2007)
46. Wang, D, Zhao, J, Chen, B, Zhu, C: Lattice vibration fundamentals in nanocrystalline anatase investigated with Raman scattering. J Phys Condens Matter **20**, 085212 (2008)
47. Paul, S, Choudhury, A: Investigation of the optical property and photocatalytic activity of mixed phase nanocrystalline titania. Appl Nanoscience **20** (2008). doi:10.1007/s13204-013-0264-3
48. Lei, S, Duan, W: Highly active mixed-phase TiO_2 photocatalysts fabricated at low temperature and the correlation between phase composition and photocatalytic activity. J Environ Sci **20**, 1263–1267 (2008)